# Top Quark Mass Calibration for Monte Carlo Event Generators

Mathias Butenschoen,[1,*] Bahman Dehnadi,[2,†] André H. Hoang,[2,3,‡] Vicent Mateu,[4,§] Moritz Preisser,[2,‖] and Iain W. Stewart[5,¶]

[1]*II. Institut für Theoretische Physik, Universität Hamburg, Luruper Chaussee 149, D-22761 Hamburg, Germany*
[2]*University of Vienna, Faculty of Physics, Boltzmanngasse 5, A-1090 Wien, Austria*
[3]*Erwin Schrödinger International Institute for Mathematical Physics, University of Vienna, Boltzmanngasse 9, A-1090 Wien, Austria*
[4]*Departamento de Física Teórica and Instituto de Física Teórica, IFT-UAM/CSIC, Universidad Autónoma de Madrid, Cantoblanco, 28049 Madrid, Spain*
[5]*Center for Theoretical Physics, Massachusetts Institute of Technology, Cambridge, Massachusetts 02139, USA*

(Received 19 August 2016; published 29 November 2016)

The most precise top quark mass measurements use kinematic reconstruction methods, determining the top mass parameter of a Monte Carlo event generator $m_t^{\rm MC}$. Because of hadronization and parton-shower dynamics, relating $m_t^{\rm MC}$ to a field theory mass is difficult. We present a calibration procedure to determine this relation using hadron level QCD predictions for observables with kinematic mass sensitivity. Fitting $e^+e^-$ 2-jettiness calculations at next-to-leading-logarithmic and next-to-next-to-leading-logarithmic order to PYTHIA 8.205, $m_t^{\rm MC}$ differs from the pole mass by 900 and 600 MeV, respectively, and agrees with the MSR mass within uncertainties, $m_t^{\rm MC} \simeq m_{t,1\,\rm GeV}^{\rm MSR}$.

DOI: 10.1103/PhysRevLett.117.232001

Making more precise measurements of Standard Model parameters is a major aim of the collider physics program. The determination of the top quark mass is important due to its influence on many quantitative and conceptual aspects for the Standard Model and beyond. The most precise determinations to date include the combined result from the Tevatron $m_t = 174.34(64)$ GeV [1], CMS Run-I $m_t = 172.44(49)$ GeV [2], and ATLAS Run-I $m_t = 172.84(70)$ GeV [3].

The highest precision measurements are based on direct reconstruction methods exploiting kinematic properties related to the top quark mass, and are based on multivariate fits that depend on a maximum amount of information on the top decay final states. This includes template and matrix element fits for distributions such as the measured invariant mass. These observables are highly differential, depending on experimental cuts and jet dynamics. Multipurpose Monte Carlo (MC) event generators are employed to do the analysis, and the results are influenced by both perturbative and nonperturbative QCD effects. Thus, the measured mass is the top mass parameter $m_t^{\rm MC}$ contained in the particular MC event generator. Its interpretation may also depend in part on the MC tuning and the observables used in the analysis.

The systematic uncertainties from MC modeling are a dominant uncertainty in the above measurements, but do not address how $m_t^{\rm MC}$ is related to a mass parameter defined precisely in quantum field theory that can be globally used for higher-order predictions. The relation is nontrivial because it requires an understanding of the interplay between the partonic components of the MC generator (hard matrix elements and parton shower) and the hadronization model. In the context of top quark mass determinations, it is often assumed that MC generators should be considered as models whose partonic components and hadronization models are, through the tuning procedure, capable of describing experimental data to a precision that is higher than that of their partonic input.

In the past $m_t^{\rm MC}$ has been frequently identified with the pole mass. This is compatible with parton-shower implementations for massive quarks, but a direct identification is disfavored because of sensitivity to nonperturbative effects from below the MC shower cutoff, $\Lambda_c \sim 1$ GeV. Also, the pole mass has an $\mathcal{O}(\Lambda_{\rm QCD})$ renormalon ambiguity, while $m_t^{\rm MC}$ does not (since partonic information is not employed below $\Lambda_c$). It has been argued [4,5] that $m_t^{\rm MC}$ has a closer relation to the MSR mass $m_t^{\rm MSR}(R \approx \Lambda_c)$, where the scale $R$ defining this scheme is close to $\Lambda_c$. The MSR mass $m_t^{\rm MSR}(R)$ [6] applies the pole mass subtraction for momentum fluctuations only from above $R$ and also does not suffer from the renormalon ambiguity.

For a given MC generator, $m_t^{\rm MC}$ can be calibrated into a field theory mass scheme through a fit of MC predictions to hadron level QCD computations for observables closely related to the distributions that enter the experimental analyses. In this Letter we provide a precise quantitative study on the interpretation of $m_t^{\rm MC}$ in terms of the MSR and pole mass schemes based on a hadron level prediction for the variable $\tau_2$ for the production of a boosted top-antitop quark pair in $e^+e^-$ annihilation. It is defined as

$$\tau_2 = 1 - \max_{\vec{n}_t} \frac{\sum_i |\vec{n}_t \cdot \vec{p}_i|}{Q}, \tag{1}$$

where the sum is over the 3-momenta of all final state particles, the maximum defines the thrust axis $\vec{n}_t$, and $Q$ is the center-of-mass energy. In Refs. [7,8] a factorization theorem has been proven for boosted top quarks, yielding

 

hadron level predictions for $\tau_2$, which we refer to as 2-jettiness [9]. For unstable top quarks it is very close to thrust, which has the sum of the 3-momenta magnitudes for final states instead of $Q$ in Eq. (1). The $\tau_2$ distribution has a distinguished peak very sensitive to the top mass, and is a delta function at $\tau_2^{\min}(m_t) = 1 - \sqrt{1-4m_t^2/Q^2}$ at tree level. The peak region is dominated by dijet events where the top quarks decay inside narrow back-to-back cones and $\tau_2$ is directly related to the sum of the squared invariant masses $M_{a,b}^2$ in the two hemispheres defined by the thrust axis $\vec{n}_t$, $(\tau_2)_{\text{peak}} \approx (M_a^2 + M_b^2)/Q^2$. Thus, $\tau_2$ in the peak region is an observable with kinematic top mass sensitivity, just like those that enter the top quark mass reconstruction methods. Therefore, the results of our calibration study should provide information relevant for the interpretation of these measurements.

*2-jettiness distribution.*—The $\tau_2$ distribution in the peak region for boosted top quarks has the basic form

$$\frac{d\sigma}{d\tau_2} = \int dk \left(\frac{d\hat{\sigma}_{\text{s}}}{d\tau_2} + \frac{d\hat{\sigma}_{\text{ns}}}{d\tau_2}\right)\left(\tau_2 - \frac{k}{Q}\right) F_{\tau_2}(k) \times \left[1 + \mathcal{O}\left(\frac{\Lambda_{\text{QCD}}}{Q}, \frac{\Gamma_t}{m_t}\right)\right], \quad (2)$$

where $d\hat{\sigma}_s/d\tau_2$ contains the singular partonic QCD corrections $\alpha_s^j[\ln^k(\tau_2 - \tau_2^{\min})/(\tau_2 - \tau_2^{\min})]_+$ and $\alpha_s^j \delta(\tau_2 - \tau_2^{\min})$ in the dijet limit and $d\hat{\sigma}_{\text{ns}}/d\tau_2$ stands for the remaining partonic nonsingular QCD corrections. The shape function $F_{\tau_2}$ describes the nonperturbative effects from wide-angle soft gluon radiation [10]. The singular partonic contribution obeys a factorization theorem,

$$\begin{aligned}\frac{\mathrm{d}\hat{\sigma}_{\text{s}}}{\mathrm{d}\tau_2} &= Q H_Q^{(6)}(Q,\mu_Q) U_{H_Q}^{(6)}(Q,\mu_Q,\mu_m) \\ &\times H_m^{(6)}(Q,m_t,\mu_m) U_{H_m}^{(5)}\left(\frac{Q}{m_t},\mu_m,\mu_B\right) \\ &\times \int \mathrm{d}s \int \mathrm{d}k J_{B,\tau_2}^{(5)}\left(\frac{s}{m_t},\mu_B,\Gamma_t,\delta m_t\right) \\ &\times U_S^{(5)}(k,\mu_B,\mu_S)\, \hat{S}_{\tau_2}^{(5)}\left(Q[\tau_2 - \tau_2^{\min}(m_t)] - \frac{s}{Q} - k, \mu_S\right), \end{aligned} \quad (3)$$

based on Soft-Collinear Effective Theory [11–14], which separates the contributions from the hard interactions in the hard functions $H_Q$ and $H_m$, the jet function $J_{B,\tau_2}$, and the soft cross talk between the top and antitop jets in the partonic soft function $\hat{S}_{\tau_2}$. The jet function $J_{B,\tau_2}$ is derived in boosted heavy quark effective theory [7] since the collinear top jet invariant mass in the peak region is very close to the top quark mass. It includes the collinear dynamics of the decaying top quarks and leading top finite-width effects. The various evolution factors $U_X$ sum large logarithms.

Results for $d\hat{\sigma}_s/d\tau_2$ with next-to-leading logarithmic resummation + $\mathcal{O}(\alpha_s)$ singular corrections (NLL + NLO) can be found in Ref. [8], with the addition of the virtual top quark contribution and rapidity logarithms in $H_m$ and $U_{H_m}$ from Ref. [15]. The next-to-next-to-leading logarithmic (NNLL) evolution in $U_{H_Q}$ and $U_S$ is known from the massless quark case, and is consistent with the direct $\mathcal{O}(\alpha_s^2)$ calculation of the $J_{B,\tau_2}$ anomalous dimension [16]. We implemented all the NNLL order ingredients for the proper treatment of the flavor number dependence [superscript (6) for including top as dynamic quark versus superscript (5) for excluding the top] in the RG evolution [17,18]. We also include the $\mathcal{O}(\alpha_s)$ nonsingular corrections $d\hat{\sigma}_{\text{ns}}/d\tau_2$ [19].

For the shape function $F_{\tau_2}$ we use the convergent basis functions introduced in Ref. [20] truncated to 4 elements (where the fourth element is already numerically irrelevant). These elements determine moments of the shape function $\Omega_i$ [21,22], which are the parameters that can also be fit together with $\alpha_s$ in event-shape analyses [21–28]. The leading power correction $\Omega_1$ is defined in the $R$-gap scheme such that it cancels an $\mathcal{O}(\Lambda_{\text{QCD}})$ renormalon present in $\hat{S}_{\tau_2}$ [29]. This is achieved through an appropriate subtraction series $\delta(R_S, \mu_S)$ [30], which induces both $R_S$ and $\mu_S$ dependence in $\Omega_1$. We quote results for $\Omega_1$ at the reference scales $\mu_S = R_S = 2$ GeV. The evolution of $\Omega_1$ with $R_S$ is described by $R$-evolution [6,31].

Equation (3) is written in terms of a generic mass scheme $m_t$, with $\delta m_t = m_t^{\text{pole}} - m_t$ in $J_{B,\tau_2}^{(5)}$ controlling the dominant sensitivity to the mass scheme. In the pole mass scheme, $\delta m_t = 0$. Using renormalon-free schemes, the $\overline{\text{MS}}$ mass with $\delta m_t \propto m_t$ is appropriate for the hard functions. In the jet function $J_{B,\tau_2}^{(5)}$ one has to adopt a scheme such as MSR [6] with $\delta m_t \sim R \sim \Gamma_t$ to maintain the power counting in the peak region. The MSR scheme is defined by $[a \equiv \alpha_s^{(5)}(R)/4\pi]$

$$m_t^{\text{pole}} - m_t^{\text{MSR}}(R) \equiv R(c_1 a + c_2 a^2 + c_3 a^3 + \cdots), \quad (4)$$

where $c_1 = 5.333$, $c_2 = 131.785$, $c_3 = 4699.703, \ldots$ are precisely the coefficients that define the series relating the $\overline{\text{MS}}$ to pole mass, $m_t^{\text{pole}} - \overline{m}_t(\overline{m}_t)$ with $R = \overline{m}_t(\overline{m}_t)$. The evolution of the MSR mass with $R$ is also described by $R$-evolution. The MSR mass is convenient as it is directly related to the $\overline{\text{MS}}$ mass, $m_t^{\text{MSR}}(\overline{m}_t) = \overline{m}_t(\overline{m}_t)$. Because of $\lim_{R\to 0} m_t^{\text{MSR}}(R) = m_t^{\text{pole}}$ it interpolates to the pole mass. However, in taking this limit one encounters the Landau singularity reflecting the pole mass renormalon problem.

To sum large logarithms we use $\tau_2$-dependent scales $\mu_i(\tau_2)$ and $R_i(\tau_2)$, known as profile functions [20,21]. They have canonical scaling in resummation regions, freeze at a perturbative scale to avoid the Landau pole, and exhibit smooth transitions between regions. They are expressed in terms of 9 parameters that are varied to estimate perturbative uncertainties. We developed a natural generalization of those used for massless event shapes in Ref. [32], to which they reduce in the massless limit [19].

For a given center-of-mass energy $Q$, the key parameters that enter the QCD factorization predictions for the $\tau_2$ distribution are the top mass $m_t$, the top width $\Gamma_t$, the hadronic parameters $\Omega_i$, and the strong coupling $\alpha_s(m_Z)$. We will consider fits both in the pole and the MSR mass schemes. Our results in the MSR scheme are given in terms of $m_t^{\rm MSR}(1\ {\rm GeV})$ following Refs. [4,5].

*Fit procedure.*—For a given $m_t^{\rm MC}$, we produce MC data sets for $d\sigma/d\tau_2$ in the peak region for various $Q$ values. For a given profile and value of $\alpha_s(m_Z)$, we fit the parameters $m_t$ and $\Omega_i$ of the hadron level QCD predictions to this MC data set. We fit for integrals over bins in $\tau_2$ of size $\simeq 0.13\ {\rm GeV}/Q$. For each $Q$ value the distribution is normalized over the fit range, and multiple $Q$'s are needed simultaneously to break degeneracies. This procedure is carried out for the MC output and the QCD predictions. We then construct the $\chi^2$ using the statistical uncertainties in the MC data sets. We do the fit by first, for a given value of $m_t$, minimizing $\chi^2$ with respect to the $\Omega_i$ parameters. The resulting marginalized $\chi^2$ is then minimized with respect to $m_t$ used in the QCD predictions. Uncertainties obtained for the QCD parameters from this $\chi^2$ simply reflect the MC statistical uncertainties used to construct the $\chi^2$. When fitting for $m_t^{\rm pole}$ or $m_t^{\rm MSR}(1\ {\rm GeV})$, we find that the resulting $\chi^2$ is no longer sensitive to $\alpha_s(m_Z)$. Therefore, we fix $\alpha_s(m_Z)$ to the world average, and do not consider it as a fit parameter.

To estimate the perturbative uncertainty in the QCD predictions we take 500 random points in the profile-function parameter space and perform a fit for each of them. The 500 sets of best-fit values provide an ensemble from which we remove the upper and lower 1.5% in the mass values to eliminate potential numerical outliers. From the ensemble we determine central values from the average of the largest and smallest values and perturbative uncertainties from half the covered interval.

To illustrate the calibration procedure we use PYTHIA 8.205 [33,34] with the $e^+e^-$ default tune 7 (the Monash 2013 tune [35] for which $\Lambda_c = 0.5$ GeV) for top mass parameter values $m_t^{\rm MC} = 170$, 171, 172, 173, 174, and 175 GeV. We use a fixed top quark width $\Gamma_t = 1.4$ GeV, which is independent of $m_t^{\rm MC}$. (Final calibration results for an $m_t^{\rm MC}$-dependent top width differ by less than 25 MeV). No other changes are made to the default settings. To minimize statistical uncertainties, we generate each distribution with $10^7$ events. We have carried out fits for the following seven $Q$ sets (in GeV units): (600,1000,1400), (700,1000,1400), (800,1000,1400), (600–900), (600–1400), (700–1000), and (700–1400), where the ranges refer to steps of 100. For each one of these sets we have considered three ranges of $\tau_2$ in the peak region: (60%, 80%), (70%, 80%), and (80%, 80%), where ($x$%, $y$%) means that we include regions of the spectra for $\tau_2 < \tau_2^{\rm peak}$ with cross section values larger than $x$% of the peak height, and $\tau_2 > \tau_2^{\rm peak}$ with cross sections larger than $y$% of the peak height, where $\tau_2^{\rm peak}$ is the peak position. This makes a total of 21 fit settings, each of which gives central values and scale uncertainties for the top mass and the $\Omega_i$.

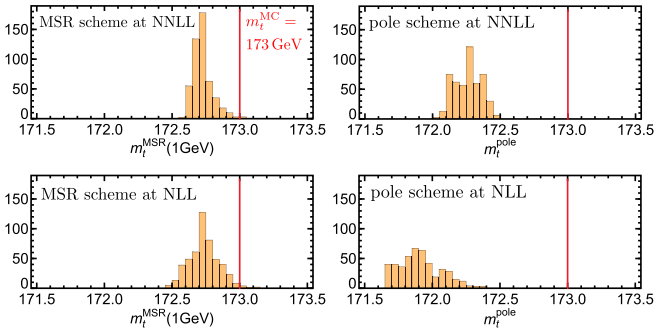


FIG. 1. Distribution of best-fit mass values from the scan over parameters describing perturbative uncertainties. Results are shown for cross sections employing the MSR mass $m_t^{\rm MSR}(1\ {\rm GeV})$ (top two panels) and the pole mass $m_t^{\rm pole}$ (bottom two panels), both at NNLL and NLL. The PYTHIA data sets use $m_t^{\rm MC} = 173$ GeV as an input (vertical red lines).

*Numerical results of the calibration.*—To visualize the stability of our fits, we display in Fig. 1 the distribution of best-fit mass values obtained for 500 random profile functions for $m_t^{\rm MC} = 173$ GeV based on the $Q$ set (600–1400) and the bin range (60%, 80%). Results are shown for $m_t^{\rm MSR}(1\ {\rm GeV})$ and $m_t^{\rm pole}$ at NLL and NNLL order, exhibiting good convergence, with the higher-order result having a smaller perturbative scale uncertainty. The results for $m_t^{\rm MSR}(1\ {\rm GeV})$ are stable and about 200 MeV below $m_t^{\rm MC}$, confirming the close relation of $m_t^{\rm MSR}(1\ {\rm GeV})$ and $m_t^{\rm MC}$ suggested in Refs. [4,5]. We observe that $m_t^{\rm pole}$ is about 1.1 GeV (NLL) and 0.7 GeV (NNLL) lower than $m_t^{\rm MC}$, demonstrating that corrections here are bigger, and that the MC mass cannot simply be identified with the pole mass. These fit results are compatible with converting $m_t^{\rm MSR}$ with $R \simeq \mu_B \simeq \mu_S Q/m_t \simeq 10\,{\rm GeV}$ to $m_t^{\rm pole}$ using Eq. (4), where $\mu_B$ is the renormalization scale of the jet function $J_{B,\tau_2}$ which governs the dominant mass sensitivity. In Fig. 2 we see the level of agreement between the MC and theory results in the MSR scheme at NNLL order for this fit. The bands show the NNLL perturbative uncertainty from the profile variations.

The results from the fits to the 21 different $Q$ sets and bin ranges mentioned above are quite similar. The differences can be associated to the level of incompatibility of the MC event generator results to the QCD predictions, and unlike the perturbative uncertainties, these differences need not necessarily decrease when going from NLL to NNLL. We will use the differences from the 21 fits to assign an additional *incompatibility uncertainty* between QCD and the MC generator for the calibration.

To quote final results we use the following procedure: (1) Take the average of the highest and lowest central values from the 21 sets as the final central value of our calibration. (2) Take the average of the scale uncertainties of these sets as our final estimate for the perturbative

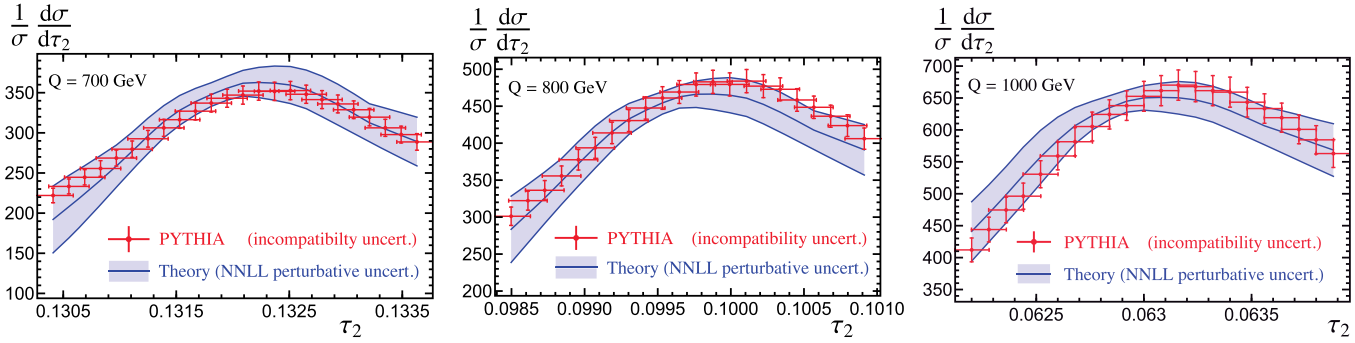


FIG. 2. Comparison of PYTHIA samples with $10^7$ events and $m_t^{\mathrm{MC}} = 173$ GeV (red dots) to the theoretical prediction in the MSR scheme at NNLL for $m_t^{\mathrm{MSR}}(1\ \mathrm{GeV}) = 172.81$ GeV and $\Omega_1 = 0.44$ GeV. The blue band shows the perturbative uncertainty from a random scan over 500 profile functions. Vertical error bars on the PYTHIA points are obtained by a global rescaling of PYTHIA statistical uncertainties such that the average $\chi^2_{\mathrm{min}}/\mathrm{dof} = 1$ and roughly indicate the incompatibility uncertainties on the cross sections. Horizontal error bars are related to the N$^2$LL incompatibility uncertainty in the MSR mass shown in Table I.

uncertainty. (3) Take half of the difference of the largest and smallest central values from the sets as the incompatibility uncertainty. (4) Quadratically add the perturbative and incompatibility errors to obtain a final uncertainty.

Using $\alpha_s$ values within the uncertainty of the world average $\alpha_s(m_Z) = 0.1181(13)$ gives an additional parametric uncertainty of $\simeq 20$ MeV for $m_t^{\mathrm{MSR}}(1\ \mathrm{GeV})$ and $m_t^{\mathrm{pole}}$ at NNLL order. This is an order of magnitude smaller than the other uncertainties and we therefore neglect it.

Table I shows our final results for the MSR mass $m_t^{\mathrm{MSR}}(1\ \mathrm{GeV})$ and $m_t^{\mathrm{pole}}$ at NLL and NNLL order, utilizing the $m_t^{\mathrm{MC}} = 173$ GeV data set. For $m_t^{\mathrm{MSR}}(1\ \mathrm{GeV})$ we observe a reduction of perturbative uncertainties from 260 MeV at NLL to 190 MeV at NNLL. The corresponding incompatibility uncertainties are 140 and 110 MeV. The corresponding fit results for the first shape function moment are $\Omega_1^{\mathrm{PY}} = 0.42 \pm 0.07 \pm 0.03$ GeV at NNLL and $\Omega_1^{\mathrm{PY}} = 0.41 \pm 0.07 \pm 0.02$ GeV at NLL order with the first uncertainty coming from scale variation and the second from incompatibility. The result agrees nicely with the expectation that $\Omega_1 \sim \Lambda_{\mathrm{QCD}}$. For $m_t^{\mathrm{pole}}$ there is a significant difference to $m_t^{\mathrm{MC}}$, and we observe that the central value shifts by 330 MeV between NLL and NNLL order. There is a reduction of perturbative uncertainties like in the MSR scheme; however, the incompatibility uncertainty increases at NNLL order. These results may not be unexpected, since the pole mass often leads to poor convergence of perturbative series.

TABLE I. Results of the calibration for $m_t^{\mathrm{MC}} = 173$ GeV in PYTHIA, combining results from all $Q$ sets and bin ranges. Shown are central values, perturbative and incompatibility uncertainties, and the total uncertainty, all in GeV.

| $m_t^{\mathrm{MC}} = 173$ GeV $(\tau_2^{e^+e^-})$ | | | | | |
|---|---|---|---|---|---|
| Mass | Order | Central | Perturb. | Incompatibility | Total |
| $m_{t,1\ \mathrm{GeV}}^{\mathrm{MSR}}$ | NLL | 172.80 | 0.26 | 0.14 | 0.29 |
| $m_{t,1\ \mathrm{GeV}}^{\mathrm{MSR}}$ | NNLL | 172.82 | 0.19 | 0.11 | 0.22 |
| $m_t^{\mathrm{pole}}$ | NLL | 172.10 | 0.34 | 0.16 | 0.38 |
| $m_t^{\mathrm{pole}}$ | NNLL | 172.43 | 0.18 | 0.22 | 0.28 |

Figure 3 shows the outcome of our fits for the MSR mass $m_t^{\mathrm{MSR}}(1\ \mathrm{GeV})$ at NNLL order with six different input values for $m_t^{\mathrm{MC}}$, and error bars with the total uncertainties. We see the expected strong correlation between these masses. This calibration results in Table I and Fig. 3 should be independently determined for each MC and each generator setting (such as different tunes).

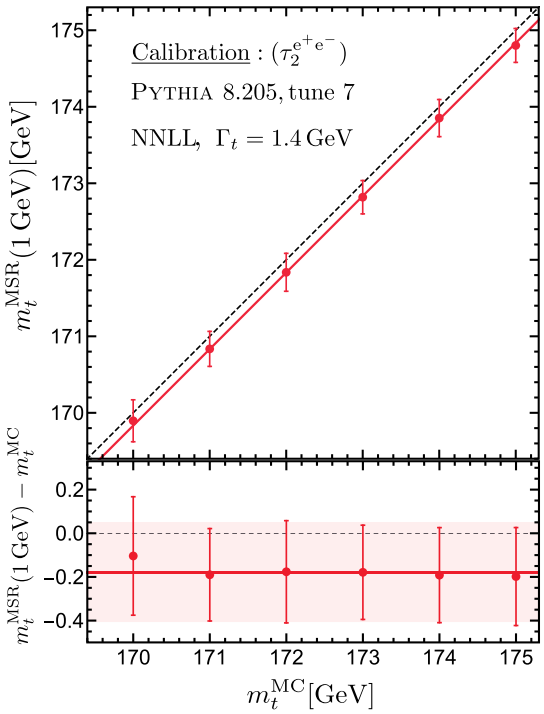


FIG. 3. Dependence of the NNLL fit result for the MSR mass on the input $m_t^{\mathrm{MC}}$ value in PYTHIA. The error bars show the total calibration uncertainty. The red solid lines correspond to the weighted average of the individual results. The red shaded area shows the average of the individual uncertainties.

To the extent that the treatment of the top factorizes for different kinematically sensitive observables both in MC generators and in QCD, and from whether one considers $e^+e^-$ or $pp$ collisions, our method can be used to calibrate $m_t^{\mathrm{MC}}$ in current experimental reconstruction analyses. $pp$ collisions introduce initial state radiation, color reconnection, and additional hadronization and multiparton interaction effects not present in $e^+e^-$. In the future our method can be extended to use other $e^+e^-$ and also $pp$ observables to directly study these effects and also the universality of the calibration procedure. Prior to this, we believe that applying our $e^+e^-$ calibration to $m_t^{\mathrm{MC}}$ from a typical $pp$ reconstruction analysis will give a more accurate result than assuming $m_t^{\mathrm{MC}} = m_t^{\mathrm{pole}}$. When corresponding hadron level predictions exist, this calibration procedure can also be applied to other MC parameters. The calibration procedure may also provide new ways to test and improve MC event generators.

We thank Marcel Vos, Peter Skands, Torbjörn Sjöstrand, Juan Fuster, and Frank Tackmann for numerous discussions. We acknowledge partial support by the FWF Austrian Science Fund under the Doctoral Program No. W1252-N27 and Project No. P28535-N27, the Spanish MINECO Ramón y Cajal Program No. (RYC-2014-16022), the U.S. Department of Energy under Grant No. DE-SC0011090, and the Simons Foundation through Grant No. 327942. We thank the Erwin Schrödinger International Institute for Mathematics and Physics, the University of Vienna and Cultural Section of the City of Vienna (MA7) for partial support.

*mathias.butenschoen@desy.de
†bahman.dehnadi@univie.ac.at
‡andre.hoang@univie.ac.at
§vicent.mateu@uam.es
‖moritz.preisser@univie.ac.at
¶iains@mit.edu

[1] CDF and D0 Collaborations (Tevatron Electroweak Working Group), Combination of CDF and D0 results on the mass of the top quark using up to 9.7 fb$^{-1}$ at the Tevatron, arXiv:1407.2682.
[2] V. Khachatryan *et al.* (CMS Collaboration), Measurement of the top quark mass using proton-proton data at $\sqrt{(s)} = 7$ and 8 TeV, Phys. Rev. D **93**, 072004 (2016).
[3] M. Aaboud *et al.* (ATLAS Collaboration), Measurement of the top quark mass in the $t\bar{t} \to$ dilepton channel from $\sqrt{s} = 8$ TeV ATLAS data, Phys. Lett. B **761**, 350 (2016).
[4] A. H. Hoang and I. W. Stewart, Top mass measurements from jets and the tevatron top-quark mass, Nucl. Phys. B, Proc. Suppl. **185**, 220 (2008).
[5] A. H. Hoang, The top mass: Interpretation and theoretical uncertainties, arXiv:1412.3649.
[6] A. H. Hoang, A. Jain, I. Scimemi, and I. W. Stewart, Infrared Renormalization Group Flow for Heavy Quark Masses, Phys. Rev. Lett. **101**, 151602 (2008).
[7] S. Fleming, A. H. Hoang, S. Mantry, and I. W. Stewart, Jets from massive unstable particles: Top-mass determination, Phys. Rev. D **77**, 074010 (2008).
[8] S. Fleming, A. H. Hoang, S. Mantry, and I. W. Stewart, Top jets in the peak region: Factorization analysis with NLL resummation, Phys. Rev. D **77**, 114003 (2008).
[9] I. W. Stewart, F. J. Tackmann, and W. J. Waalewijn, N-Jettiness: An Inclusive Event Shape to Veto Jets, Phys. Rev. Lett. **105**, 092002 (2010).
[10] G. P. Korchemsky and G. Sterman, Power corrections to event shapes and factorization, Nucl. Phys. **B555**, 335 (1999).
[11] C. W. Bauer, S. Fleming, and M. Luke, Summing Sudakov logarithms in $B \to X_s\gamma$ in effective field theory, Phys. Rev. D **63**, 014006 (2000).
[12] C. W. Bauer, S. Fleming, D. Pirjol, and I. W. Stewart, An effective field theory for collinear and soft gluons: Heavy to light decays, Phys. Rev. D **63**, 114020 (2001).
[13] C. W. Bauer and I. W. Stewart, Invariant operators in collinear effective theory, Phys. Lett. B **516**, 134 (2001).
[14] C. W. Bauer, D. Pirjol, and I. W. Stewart, Soft-collinear factorization in effective field theory, Phys. Rev. D **65**, 054022 (2002).
[15] A. H. Hoang, A. Pathak, P. Pietrulewicz, and I. W. Stewart, Hard matching for boosted tops at two loops, J. High Energy Phys. 12 (2015) 059.
[16] A. Jain, I. Scimemi, and I. W. Stewart, Two-loop jet-function and jet-mass for top quarks, Phys. Rev. D **77**, 094008 (2008).
[17] S. Gritschacher, A. H. Hoang, I. Jemos, and P. Pietrulewicz, Secondary heavy quark production in jets through mass modes, Phys. Rev. D **88**, 034021 (2013).
[18] P. Pietrulewicz, S. Gritschacher, A. H. Hoang, I. Jemos, and V. Mateu, Variable flavor number scheme for final state jets in thrust, Phys. Rev. D **90**, 114001 (2014).
[19] B. Dehnadi, Heavy quark mass determinations with sum rules and jets, Ph.D. thesis, University of Vienna, 2016.
[20] Z. Ligeti, I. W. Stewart, and F. J. Tackmann, Treating the $b$ quark distribution function with reliable uncertainties, Phys. Rev. D **78**, 114014 (2008).
[21] R. Abbate, M. Fickinger, A. H. Hoang, V. Mateu, and I. W. Stewart, Thrust at N$^3$LL with power corrections and a precision global fit for $\alpha_s(m_Z)$, Phys. Rev. D **83**, 074021 (2011).
[22] R. Abbate, M. Fickinger, A. H. Hoang, V. Mateu, and I. W. Stewart, Precision thrust cumulant moments at N$^3$LL, Phys. Rev. D **86**, 094002 (2012).
[23] T. Becher and M. D. Schwartz, A precise determination of $\alpha_s$ from LEP thrust data using effective field theory, J. High Energy Phys. 07 (2008) 034.
[24] R. A. Davison and B. R. Webber, Non-perturbative contribution to the thrust distribution in $e^+e^-$ annihilation, Eur. Phys. J. C **59**, 13 (2009).
[25] T. Gehrmann, M. Jaquier, and G. Luisoni, Hadronization effects in event shape moments, Eur. Phys. J. C **67**, 57 (2010).
[26] Y.-T. Chien and M. D. Schwartz, Resummation of heavy jet mass and comparison to LEP data, J. High Energy Phys. 08 (2010) 058.
[27] T. Gehrmann, G. Luisoni, and P. F. Monni, Power corrections in the dispersive model for a determination of the

strong coupling constant from the thrust distribution, Eur. Phys. J. C **73**, 2265 (2013).
[28] A. H. Hoang, D. W. Kolodrubetz, V. Mateu, and I. W. Stewart, Precise determination of $\alpha_s$ from the $C$-parameter distribution, Phys. Rev. D **91**, 094018 (2015).
[29] A. H. Hoang and I. W. Stewart, Designing gapped soft functions for jet production, Phys. Lett. B **660**, 483 (2008).
[30] A. H. Hoang and S. Kluth, Hemisphere soft function at $O(\alpha_s^2)$ for dijet production in $e^+e^-$ annihilation, arXiv:0806.3852.
[31] A. H. Hoang, A. Jain, I. Scimemi, and I. W. Stewart, R-evolution: Improving perturbative QCD, Phys. Rev. D **82**, 011501 (2010).
[32] A. H. Hoang, D. W. Kolodrubetz, V. Mateu, and I. W. Stewart, $C$-parameter distribution at $N^3LL'$ including power corrections, Phys. Rev. D **91**, 094017 (2015).
[33] T. Sjöstrand, S. Mrenna, and P. Z. Skands, PYTHIA 6.4 physics and manual, J. High Energy Phys. 05 (2006) 026.
[34] T. Sjöstrand, S. Ask, J. R. Christiansen, R. Corke, N. Desai, P. Ilten, S. Mrenna, S. Prestel, C. O. Rasmussen, and P. Z. Skands, An introduction to PYTHIA 8.2, Comput. Phys. Commun. **191**, 159 (2015).
[35] P. Skands, S. Carrazza, and J. Rojo, Tuning PYTHIA 8.1: the Monash 2013 Tune, Eur. Phys. J. C **74**, 3024 (2014).